

Appendix. Table I: Ship parameters

Description	Parameter	Full-scale	Scaling
Ship length	$L_{pp}$	230m	7.2786m
Ship breadth	$B$	32.2m	1.019m
Ship height	$D$	19m	0.6013m
Ship draft	$T$	10.8m	0.3418m
Block coefficient	$C_b$	0.6505	0.6505
Nominal Froude number	$F_r$	0.26	0.26
Nominal navigation speed	$U$	24.6 kn	2.196 m/s
Displacement	—	52055 ton	1.6497

## I. CONSTRAINTS

The SOC constraint is formulated by Appendix.equation(1).

$$\begin{cases} I_{min}^{char,SOC}(k) = \frac{SOC_{bat}(k) - SOC_{bat}^{max}}{\eta_i \Delta T / C_{bat}(k)} \\ I_{min}^{dis,SOC}(k) = \frac{SOC_{bat}(k) - SOC_{bat}^{min}}{\eta_i \Delta T / C_{bat}(k)} \end{cases} \quad (1)$$

where,  $I_{min}^{char,SOC}$  and  $I_{min}^{dis,SOC}$  are the minimum and maximum current range of battery based on SOC constraint, respectively;  $SOC_{bat}^{max}$  and  $SOC_{bat}^{min}$  are the maximum and minimum SOC ranges of battery, respectively.

In the voltage constraint, the voltage boundary to prevent the battery terminal voltage from exceeding the safe voltage range, i.e., the minimum voltage  $U_{bat}^{min}$  and the maximum voltage  $U_{bat}^{max}$  of battery, shown in Appendix. equation (2).

$$\begin{cases} U_{bat}^{min}(k) = OCV(k) - U_p(k) - R_0(k)I_{max}^{dis,vol}(k) \\ U_{bat}^{max}(k) = OCV(k) - U_p(k) - R_0(k)I_{min}^{char,vol}(k) \\ OCV(k) = [OCV - \frac{\eta_i \Delta T}{C_{bat}} \frac{\partial OCV}{\partial SOC_{bat}} I_{bat}]|_{k-1} \end{cases} \quad (2)$$

where,  $I_{min}^{char,vol}$  and  $I_{max}^{dis,vol}$  are the minimum pulse current and the maximum pulse current caused by the voltage boundary, shown in Appendix. equation(3).

$$\begin{cases} I_{min}^{char,vol}(k) = \frac{OCV - U_p e^{-\Delta t/\tau} - U_{bat,max}}{\frac{\eta_i \Delta t}{C_{bat}} \frac{\partial OCV}{\partial SOC_{bat}} + R_p(1 - e^{-\Delta t/\tau}) + R_0}|_k \\ I_{max}^{dis,vol}(k) = \frac{OCV - U_p e^{-\Delta t/\tau} - U_{bat,min}}{\frac{\eta_i \Delta t}{C_{bat}} \frac{\partial OCV}{\partial SOC_{bat}} + R_p(1 - e^{-\Delta t/\tau}) + R_0}|_k \end{cases} \quad (3)$$

## II. SOLUTION PROCESS AND STABILITY ANALYSIS

The error augmentation model of HESS is as follows:

$$\begin{cases} x(k+1) = Ax(k) + Bu(k) \\ y(k) = Cx(k) + Du(k) + Eu^2(k) + F \end{cases} \quad (4)$$

$A, B, C, D, E$  are the coefficient matrix, as flows:

$$\begin{cases} A = diag[1, 1, 1, 1] \\ B = diag[-\frac{\eta_{bat}}{3600C_{bat}(k)}, -\frac{\eta_{uc}}{U_{sc}^{oc}C_{sc}}, -\frac{\eta_{bat}}{3600C_{bat}(k)}, -\frac{\eta_{uc}}{U_{sc}^{oc}C_{sc}}] \\ C = diag[0, U_{uc}^{max}(k)I_{uc}(k), 0, U_{uc}^{max}(k)I_{uc}(k)] \\ D = diag[OCV(k), 0, OCV(k), 0] \\ E = diag[-R_0(k), -R_{uc}(k), -R_0(k), -R_{uc}(k)] \\ F = diag[-U_p, 0, -U_p, 0] \end{cases} \quad (5)$$

In the dynamic HESS model, because,

$$\begin{cases} rank([B, AB]) = 4 \\ rank([C, CA]^T) \neq 4 \\ rank([CB, CAB]) = 2 \end{cases} \quad (6)$$

So the system is completely state controllable but not completely observable. For this system, the output variable instead of state variables is required to be controlled. To predict and correct the power error, the PI method as an example can be used to simplify and solve for the current control loop, and the open loop transfer function is shown in Appendix.equation(7).

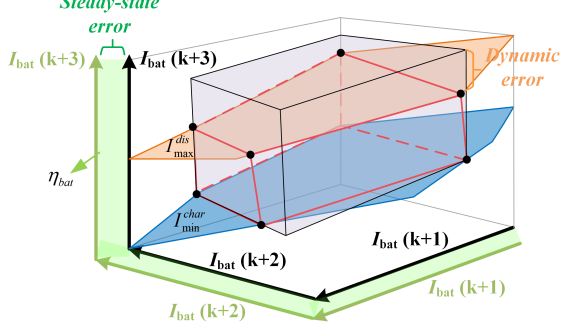
$$\left\{ \begin{array}{l} [\Delta e_{bat}(k), \Delta e_{uc}(k)] = \text{equation(35,36)} \text{ at k-th} \\ \Delta I_{bat}(k+1) = (K_{p,b} + \frac{K_{i,b}}{s}) \frac{\Delta e_{bat}(k)}{U_{bat}(k)} \\ \Delta I_{uc}(k+1) = (K_{p,c} + \frac{K_{i,c}}{s}) \frac{\Delta e_{uc}(k)}{U_{sc}(k)} \\ SOC_{bat}(k+1) = SOC_{bat}(k) \\ - \frac{\eta_{bat}}{3600C_{bat}(k)} \underbrace{(I_{bat}(k) + \Delta I_{bat}(k+1))}_{\text{Predictive: } I_{bat}(k+1)} \\ SOC_{uc}(k+1) = SOC_{uc}(k) \\ - \frac{\eta_{uc}}{U_{sc}^{oc}C_{sc}} \underbrace{(I_{uc}(k) + \Delta I_{bat}(k+1))}_{\text{Predictive: } I_{uc}(k+1)} \\ [\Delta e_{bat}(k+1), \Delta e_{uc}(k+1)] = \text{equation(35,36)} \text{ at (k+1)-th} \\ \vdots \\ (k+N_L-1). \end{array} \right. \quad (7)$$

In the  $N_L - th$  prediction interval, the state trajectory and control trajectory of HESS are obtained by Appendix.equation(8).

$$\left\{ \begin{array}{l} \begin{bmatrix} SOC_{bat}(k), SOC_{bat}(k+1), \dots, SOC_{bat}(k+N_L-1) \\ SOC_{uc}(k), SOC_{uc}(k+1), \dots, SOC_{uc}(k+N_L-1) \end{bmatrix} \\ \begin{bmatrix} I_{bat}(k), I_{bat}(k+1), \dots, I_{bat}(k+N_L-1) \\ I_{uc}(k), I_{uc}(k+1), \dots, I_{uc}(k+N_L-1) \end{bmatrix} \end{array} \right. \quad (8)$$

Considering the dynamic SOP range of the battery, an active current constraint of the battery may limit the variations of the above control trajectory, i.e.,  $[g(I_{bat})|N_{bat}I_{min}^{char} \leq I_{bat} \leq N_{bat}I_{max}^{dis}]$ . When  $N = 3$ , Appendix. Fig. 1 shows the active control constraint of the battery in  $N$  dimensions. The internal space of the hexahedron surrounded by red lines is  $g(I_{bat}) \leq 0$ , and the surface of this hexahedron represents  $g(I_{bat}) = 0$ . As every two planes of this hexahedron may not be parallel, their gradient may not be in parallel. This brings difficulties in solving the battery dynamic; therefore, the steady-state error and the dynamic error of the battery may be compensated by the ultracapacitor to reduce solution complexity while ensuring power balance.

**Theorem 1.** As the battery operation, If the SOP is constantly changing, so the current constraint / power constraint



Appendix. Fig. 1. The active control constraints in three dimensions.

is active, and the resulted  $|\Delta e_{bat}| > 0$ . In each control interval,  $\Delta e_{bat}(k+1) \neq \Delta e_{bat}(k)$ , ( $0 < k \leq N_L$ ).

*Proof.* At  $k$ -time,

$$\begin{cases} |I_{bat}^{ref}(k)| = |P_{bat}^{ref}(k)/U_{bat}(k)| > |I_{bat}(k)| \\ |\Delta e_{bat}(k)| = |I_{bat}^{ref}(k) - I_{bat}(k)| > 0 \end{cases} \quad (9)$$

where,  $i_{bat}^{ref} = \frac{P_{bat}^{ref}}{U_{bat}}$  is the current demand for battery, which from the power decomposition link.

**Theorem 2.** According to equation (12) in the paper, the state of the HESS system at each moment varies randomly and is bounded along the iteration axis, and the tracking reference trajectory of the system is also non-strict repetitive. In this mode, the control problem of HESS can be converted to a fixed point problem, to ensure the convergence of control problems, a new operator can be obtained:  $F = g(x, \dot{x}, u, k) - h(x, k) + u$ ; where,  $g(x, \dot{x}, u, k) = y$  is the function of HESS output,  $h(x, k)$  is the reference of HESS output. A control signal  $u$  can be solved by the operator within a limited period  $[0, T]$  to satisfy:  $\{F(u) = u | k \in [0, T], u_k \rightarrow u\}$ . At this point,

$$\begin{cases} [g(x, \dot{x}, u, k) - h(x, k)] \rightarrow 0 \\ \|g(x, \dot{x}, u, k) - h(x, k)\| \leq \gamma \|\Delta g(x, \dot{x}, u, k) - h(x, k)\| \end{cases} \quad (10)$$

where,  $\gamma$  is the geometric series.

### III. DESCRIPTION 7

1) *Solution process:* The extreme value of the objective function can obtain the optimal solution:  $i_{ILC}(k+1) = i_{ILC} + K_{N-1}[g(k) - h(k)]$ . At this point, the iteration relationship of error is as:  $[g(k) - h(k)] = L_N[g(k) - h(k)]$ ; where,  $K_{N-1}$  and  $L_N$  are the optimal gain matrix and the gradient, they all decrease as  $N$  increases.

According to the Karush-Kun-Tucker (KKT) conditions, if the control signal of HESS  $u^* = [I_{bat}^d, I_{uc}^d]$  is the minimum, then we can get,

$$\begin{cases} \nabla J(u^*) + \sum_k^N \lambda_j^* \nabla g_j(u^*) = 0, \\ \lambda_j^* \geq 0 \\ \lambda_j^* = 0, j \notin H(u^*) \end{cases} \quad (11)$$

The Appendix.equation (11) in the paper can be written in the following compact form:

$$\begin{cases} \min(\frac{1}{2} \lambda^T H \lambda + \lambda^T P + \frac{1}{2} \gamma^T E^{-1} \gamma) \\ H = M E^{-1} M^T \\ P = \gamma + M E^{-1} F \\ u^* = -E^{-1}(F + M^T \lambda^*) \end{cases} \quad (12)$$

Then, the inequality constrained problem can be transferred to the equality constrained problem to improve the computing efficiency, as follows:

$$\lambda^* = -(M_{act} E^{-1} M^T)^{-1} (\gamma_{act} + M_{act} E^{-1} F) \geq 0 \quad (13)$$

where,  $M_{act}$  and  $\gamma_{act}$  are the relative matrix of active constraints. Finally, the quadratic programming procedure method can be used to find the optimal solutions.

2) *Stability analysis of hybrid control system:* The transfer function of the learning algorithm is given as:

$$G_{ILC}(s) = K_{ILC} \frac{1}{1 + T_c s} \quad (14)$$

where,  $K_{ILC}$  and  $T_c$  are the gain of the ILC controller and time constant, respectively. When the control interval is  $\Delta T = 5e^{-5}s$  with  $e = 10$ . The proposed control loop  $|G_{ILC}(z)CR(z)G_I(z)|$  in the battery and the ultracapacitor are formulated by Appendix. equation(15) and Appendix. equation(16), respectively.

$$\begin{cases} K_{ILC}^{buck} \frac{5.702e^{-8}z^3 + 1.679e^{-7}z^2 - 1.695e^{-7}z - 5.545e^{-8}}{z^4 - 3.946z^3 + 5.837z^2 - 3.837z + 0.9459}, \text{ Buck mode} \\ K_{ILC}^{boost} \frac{1.026e^{-7}z^3 + 3.015e^{-7}z^2 - 3.046e^{-7}z - 9.946e^{-8}}{z^4 - 3.94z^3 + 5.819z^2 - 3.82z + 0.942}, \text{ Boost mode} \end{cases} \quad (15)$$

$$\begin{cases} K_{ILC}^{buck} \frac{2.441e^{-9}z^3 + 7.191e^{-9}z^2 - 7.257e^{-9}z - 2.375e^{-9}}{z^4 - 3.946z^3 + 5.837z^2 - 3.839z + 0.9464}, \text{ Buck mode} \\ K_{ILC}^{boost} \frac{1.844e^{-8}z^3 + 5.42e^{-8}z^2 - 5.476e^{-8}z - 1.788e^{-8}}{z^4 - 3.94z^3 + 5.819z^2 - 3.82z + 0.9402}, \text{ Boost mode} \end{cases} \quad (16)$$

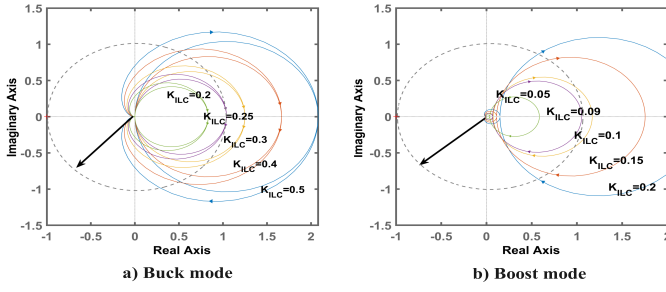
Therefore, the locus of the hybrid control system cannot exceed the unit cycle, and the associated Nyquist diagram of the battery and the ultracapacitor are shown in Appendix. Fig. 2 and Appendix. Fig. 3, respectively. To ensure the stability of the system and achieve the fast convergence of the system, the gain  $K_{ILC}^{buck}$  and  $K_{ILC}^{boost}$  of the battery are chosen as 0.25 and 0.09 by experimentation in buck mode and boost mode, respectively; the gain  $K_{ILC}^{buck}$  and  $K_{ILC}^{boost}$  of the ultracapacitor are chosen as 0.02 and 0.008 in buck mode and boost mode, respectively.

### IV. PARAMETERS

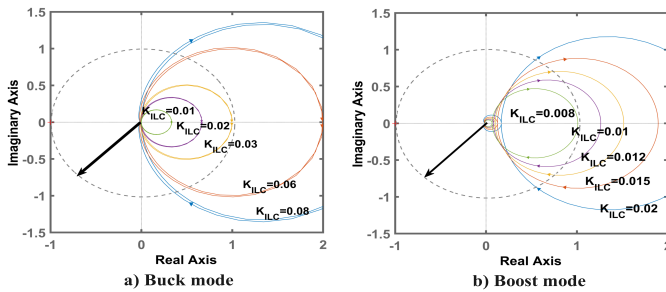
### V. RESULTS

The SOP variations of batteries under different swaying conditions are shown in Appendix. Fig. 4.

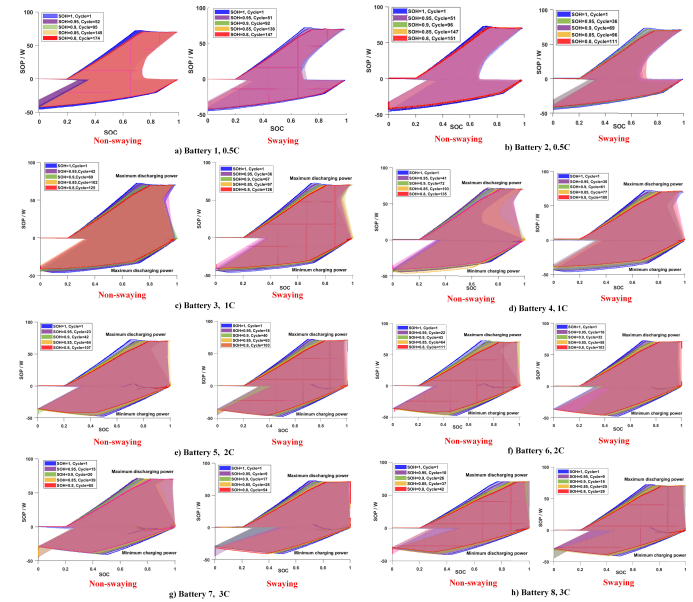
The HESS output at different initial SOCs is shown in Appendix. Fig. 5.



Appendix. Fig. 2. The locus of  $G_{ILC}(z)CR(z)G_I(z)$  of the battery.



Appendix. Fig. 3. The locus of  $G_{ILC}(z)CR(z)G_I(z)$  of the ultracapacitor.



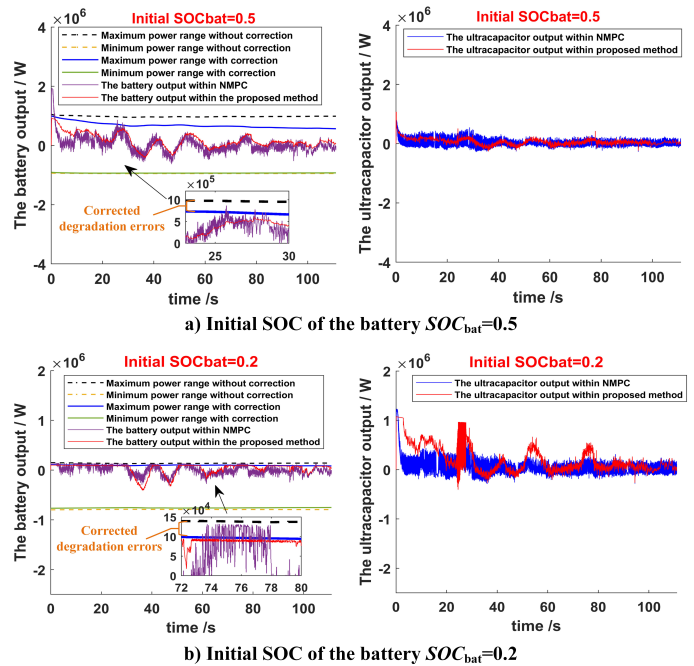
Appendix. Fig. 4. The SOP variations of batteries under different swaying conditions.

Appendix. Table II: The parameters of the tested system

Description	Value	Description	Value
Rated capacity	3350mAh	Standard charging time	4.0hours
Nominal voltage	3.6V	Maximum continuous discharge current	10A
Standard charging current	1.675A	Internal resistance	$38m\Omega$
Charging voltage	$4.20 \pm 0.03$ V	Discharging end voltage	2.5V
Current ratio of Battery1 and Battery2	0.5C	Current ratio of Battery3 and Battery4	1C
Current ratio of Battery5 and Battery6	2C	Current ratio of Battery7 and Battery8	3C

Appendix. Table III: Electrical simulation parameters

Description	Parameter	Value
No-load DC voltage	$U_{dc}^{ref}$	1500V
Initial open circuit voltage of battery	$OCV$	594 V
Capacity of battery	$C_{bat}$	1200 Ah
Initial voltage of ultracapacitor	$U_{uc}$	750 V
Capacity of ultracapacitor	$C_{uc}$	$94.5 \times 4$ F
Maximum current threshold	$I_{uc}^{max}$	2000A
Minimum current threshold	$I_{uc}^{min}$	-2000A



Appendix. Fig. 5. The variations of the HESS output.